THE JOURNAL OF PHYSICAL CHEMISTRY C

Article

Cite This: J. Phys. Chem. C 2019, 123, 3876−3885

pubs.acs.org/JPCC

Thermal Degradation of Monolayer MoS_2 on $SrTiO_3$ Supports

Peiyu Chen,*,† Wenshuo Xu,† Yakun Gao, Philip Holdway, Jamie H. Warner, and Martin R. Castell*

Department of Materials, University of Oxford, Parks Road, Oxford OX1 3PH, United Kingdom

ABSTRACT: Monolayer MoS_2 is a wide-bandgap semiconductor suitable for use in high-temperature electronics. It is therefore important to understand its thermal stability. We report the results of a study on thermal degradation of MoS_2 monolayers supported on $SrTiO_3$ substrates in ultrahigh vacuum (UHV). Our studies were carried out on the (111), (110), and (001) terminations of $SrTiO_3$ substrates, but MoS_2 was found to degrade on all of these surfaces in a similar way. By scanning tunneling microscopy, we show that MoS_2 monolayer crystals maintain their structure up to 700 °C under UHV, at which point triangular etch trenches appear along the $\langle 2\bar{1}\bar{1}0 \rangle$ lattice directions (i.e., sulfur-terminated edge directions) of the MoS_2 crystals. The trenches are due to the preferential loss of sulfur, allowing molybdenum to be oxidized by oxygen originating from the $SrTiO_3$ substrate. The intensity of the A-exciton photoluminescence (PL) peak and the E^1_{2g} and A_{1g} Raman signals reduced significantly following treatment at this temperature. The crystals continue to degrade at higher annealing temperatures in UHV until they transform into MoO_x (x = 2−3) particles at 900 °C, and the optical properties characteristic of MoS_2 are lost entirely in PL and Raman spectra. The initial sulfur loss and the formation of MoO_x are confirmed by X-ray photoelectron spectroscopy. The macroscopic triangular shapes of the MoS_2 crystals are retained until the residual particles evaporate at above 1000 °C. The optical properties of the 700 and 800 °C UHV-annealed samples can be partially recovered upon sulfur annealing. This work establishes a pathway of the thermal degradation of $SrTiO_3$-supported monolayer MoS_2 in vacuum from smooth MoS_2 crystals to crystals with sulfur vacancies (etch trenches), followed by MoO_2 and finally MoO_3 particles. We also demonstrate how sulfur annealing can be used to heal the defects.

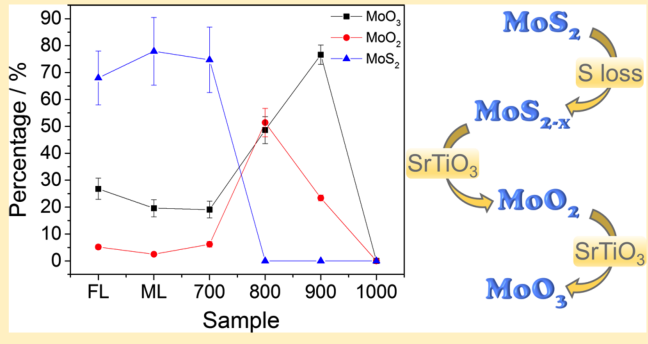

1. INTRODUCTION

Many transistors, circuits, and sensors require electronic materials that can operate at high temperatures.[1] Wide-bandgap semiconductors have been found to function effectively at elevated temperatures,[2] and increasing attention is being directed toward the use of monolayer molybdenum disulfide (MoS_2) in high-temperature applications.[1] Atomically thin MoS_2 has a direct bandgap of 1.8−1.9 eV.[3] The intense interest in this material is due to its relatively high charge mobility,[4] optical transparency, and extreme mechanical flexibility.[5] It is therefore important to understand the effects of high-temperature processing on the structure and optical properties of monolayer MoS_2.

Previous studies in this area were mostly carried out as part of the synthesis of MoS_2 or immediately after its growth. They were used to enhance the crystallinity,[6−10] optical properties,[6−8,10] or electronic properties of the MoS_2 crystals.[11,12] A few studies also explored the thermally accelerated oxidation of MoS_2 into MoO_3 under ambient conditions, starting from 100 °C until complete transformation into MoO_3 at up to 550 °C.[13−18] In these studies, the MoS_2 samples were either monolayered (ML)/few layered (FL) (supported on SiO_2) or powdered. In the absence of oxygen, MoS_2 is much more stable; the atomic structure of monolayer MoS_2 crystals on Au(111) was seen to be unperturbed up to 630 °C.[19] For FL MoS_2 crystals on oxide/nitride substrates, thermal decomposition did not occur until 850 °C in the absence of oxygen.[6] In a bulk MoS_2 crystal, S is not completely removed until above 1203 °C under vacuum.[20] Atomic force microscopy was used to determine that the oxidation of MoS_2 monolayers started with triangular pits in air.[16,17] Nevertheless, to date, there has not been a systematic report on the morphology of thermally degraded MoS_2 monolayers in vacuum. Additionally, any methods to recover the properties of degraded MoS_2 are also of significant interest.[10]

In this article, we examine the thermal decomposition in vacuum of monolayer MoS_2 supported on single crystal substrates of strontium titanate ($SrTiO_3$) terminated with (111), (110), and (001) surfaces. In contrast to most of the studies mentioned above, we exclusively study monolayer MoS_2 islands, which are of greater technological interest compared with thicker MoS_2 crystals. In vacuum, we exclude the effects of oxygen in the atmosphere so that all changes upon annealing can be attributed to MoS_2 itself and its oxide substrate. This setup allows us to assess how MoS_2 crystals would behave in devices that require high-temperature processing. We used chemical vapor deposition (CVD) to grow MoS_2 crystals, which is a scalable method that produces

Received: November 21, 2018
Revised: January 15, 2019
Published: January 15, 2019

DOI: 10.1021/acs.jpcc.8b11298
J. Phys. Chem. C 2019, 123, 3876−3885

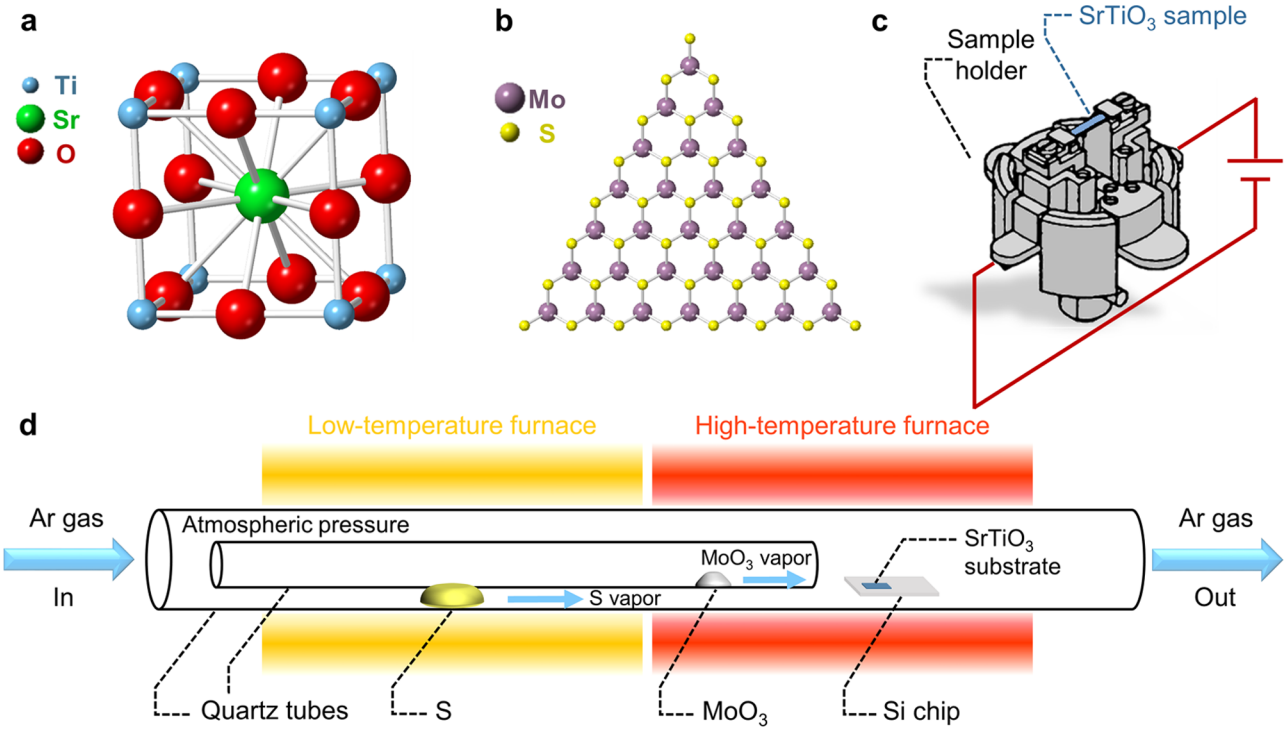

Figure 1. Crystal structures of MoS_2 and $SrTiO_3$, the UHV annealing setup, and the CVD system. (a) Cubit unit cell of $SrTiO_3$. (b) Top view of a monolayer triangular crystal of MoS_2. (c) UHV sample holder for direct resistive heating for both $SrTiO_3$ substrate preparation and the thermal annealing of MoS_2 crystals on $SrTiO_3$. (d) Schematic diagram of the CVD setup for the synthesis of MoS_2 crystals. The Si chip serves as a substrate holder.

large-area transition metal dichalcogenides of high quality. Such a growth technique is ideal for high-turnover industrial manufacturing of two-dimensional materials.

In our study, the step-by-step changes in MoS_2 monolayers were tracked from their initial degradation at 700 °C to the complete evaporation of MoO_x (x = 2−3) residues at temperatures above 1000 °C. The changes were monitored by optical microscopy (OM), scanning electron microscopy (SEM), scanning tunneling microscopy (STM), X-ray photoemission spectroscopy (XPS), photoluminescence (PL), and Raman spectroscopy. Although the optical properties of MoS_2 crystals deteriorated to a large extent after annealing in vacuum, it was found that they can be partially recovered via a follow-up annealing treatment in a sulfur atmosphere. This raises the possibility of healing any non-substantial defects via a sulfur-annealing step during the fabrication of MoS_2-based devices.

2. EXPERIMENTAL METHODS

2.1. $SrTiO_3$ Substrate Preparation. $SrTiO_3$ single crystals (7 × 2 × 0.5 mm^3) doped with niobium (Nb) at 0.5% by weight were supplied by PI-KEM, U.K., with epi-polished (111), (110), and (001) surfaces. $SrTiO_3$ is an insulator with a band gap of 3.2 eV at 25 °C.[21] The Nb dopant was included to generate sufficient electrical conductivity at room temperature for STM imaging. The substrate surfaces were studied using an ultrahigh vacuum (UHV)-STM, which is a custom-built JEOL JSTM 4500s model (base pressure 10^{-8} Pa). $SrTiO_3$ surfaces were prepared to terminate with previously well-characterized reconstructions, requiring different Ar^+-ion sputtering conditions, annealing temperatures and durations, and O_2 partial pressures.[22−24] The observation of surface reconstructions ensures that crystalline, atomically flat, and contaminant-free terminations have been achieved.

2.2. Growth of Monolayer MoS_2. The atmospheric pressure CVD method was used to grow monolayer MoS_2 crystals on the reconstructed $SrTiO_3$ substrates using the precursors molybdenum trioxide (MoO_3, powder, ≥99.5%, Sigma-Aldrich) and sulfur (S, powder, ≥99.5%, Sigma-Aldrich). The CVD setup is shown in Figure 1d. $SrTiO_3$ substrates were placed at a fixed position downstream for consistent results. The MoO_3 (20 mg) and S (450 mg) powders were loaded in a set of double-walled quartz tubes with different diameters so that the reaction region was strictly defined around the substrate surface, and their temperatures were independently controlled by two separate furnaces. After oxygen in the system was driven off by a 500 sccm argon (Ar) flow for 30 min, the S vapor at 180 °C was preintroduced by 150 sccm Ar for 15 min. This created a sulfur-rich environment, which was maintained by increasing the temperature of S at a rate of 0.7 °C s^{-1} during the synthesis. The substrates were heated up to 210 °C at the same time to avoid S condensation. The MoO_3 precursor and the $SrTiO_3$ substrates were then heated to 300 and 800 °C, respectively. There were three stages in the MoS_2 synthesis, namely, nucleation (20 min with 150 sccm Ar), main growth (25 min with 50 sccm Ar), and atom migration (15 min with 5 sccm Ar), completed by a rapid cooling process.

2.3. Thermal Annealing of Monolayer MoS_2. Following growth, the MoS_2 samples were introduced into the UHV-STM chamber for annealing. The samples were heated by resistively passing a direct current through the substrates (Figure 1c). The temperature was measured through a viewport with an optical pyrometer. The temperature was

DOI: 10.1021/acs.jpcc.8b11298
J. Phys. Chem. C 2019, 123, 3876−3885

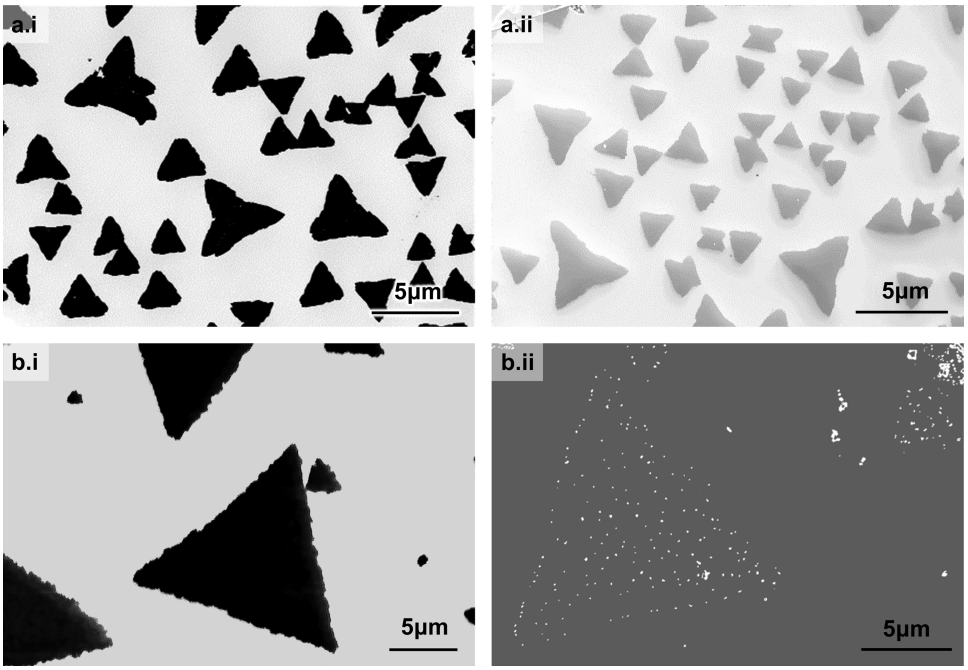

Figure 2. SEM images of MoS_2 crystals on $SrTiO_3$ substrates after UHV annealing at (a.i) 700 °C and (a.ii) 800 °C for 2 h on $SrTiO_3$(111) and (b.i) before and (b.ii) after UHV annealing at 1150 °C for 3 h on $SrTiO_3$(001). The contrast of (b.ii) is enhanced to show the residues.

ramped up and down at a rate of 2.5−5.5 °C min^{-1}, and each anneal lasted 0.5−5.5 h.

2.4. Characterization of Monolayer MoS_2. Optical microscope images of the MoS_2 crystals were taken using an Axioskop 2 MAT from Carl Zeiss Co., Ltd. SEM was performed using a Zeiss Merlin and a Hitachi-4300, both at an accelerating voltage of 3 kV. STM images were processed by Smart Align,[25,26] Gwyddion, and WSxM.[27] PL and Raman spectroscopy were conducted using a JY Horiba LabRAM ARAMIS imaging confocal Raman microscope with a 532 nm excitation wavelength and 12.5 mW laser power. The laser spot size was ∼1 μm, and the acquisition times were 5 s for PL and 35 s for Raman. XPS measurements were performed on a Thermo Scientific K-Alpha XPS instrument equipped with a microfocused monochromated Al X-ray source (1486.6 eV). The source was operated at 12 keV, and a 400 μm spot size was used. The analyzer was operated at a constant analyzer energy of 50 eV. Charge neutralization was applied using a combined low-energy/ion flood source.

2.5. Sulfur Annealing of Defective Monolayer MoS_2. The defective vacuum-annealed MoS_2 samples and sulfur powder were loaded in two quartz tubes (2 in. diameter) at the centers of two furnaces so that their temperatures could be controlled independently. After the system was flushed with a 500 sccm Ar flow for 30 min, MoS_2 and S were heated to 300 and 200 °C, respectively. The S vapor was carried by a 500 sccm Ar flow downstream to the MoS_2 sample. The S atmosphere was maintained for 1 h, after which both the MoS_2 samples and S were cooled down.

■ 3. RESULTS

Figure 1a shows a cubic unit cell of the substrate material $SrTiO_3$ with a Sr^{2+} ion (green) in the middle, Ti^{4+} ions (blue) at the corners, and the O^{2-} ions (red) along the cube edges. Previously, we reported the distinct epitaxial behavior of MoS_2 crystals on the (111), (110), and (001) substrate terminations of $SrTiO_3$[28] but here no distinct differences were noticed between their thermal stabilities on the different $SrTiO_3$ terminations. The terminations used in each case are specified in the figure captions in the remaining images of this article. Figure 1b shows the top view of a monolayer MoS_2 crystal. Figure 1c shows the UHV sample holder. This setup is used for both the high-temperature substrate preparation and the thermal annealing of MoS_2 crystals in UHV. Figure 1d shows the CVD system used to synthesize MoS_2. The sulfur annealing of defective MoS_2 crystals was carried out using the same setup without MoO_3 in the inner quartz tube.

3.1. SEM and STM Experiments. MoS_2 crystals on a $SrTiO_3$(111) substrate were annealed in UHV for 2 h with a temperature gradient across the sample. The temperature was 700 °C at the cooler end, and 800 °C at the hotter end. SEM images were taken after the sample was cooled down (Figure 2a.i,ii). The crystals at the cooler end (Figure 2a.i) are clear and black; they look no different from the as-grown crystals. Toward the hotter end, the crystals appear fainter (Figure 2a.ii). Figure 2a.ii was acquired soon after Figure 2a.i, with the same brightness and contrast settings, which means that the contrast between the MoS_2 crystals and the substrate has changed. Although the more detailed internal structure cannot be resolved by SEM, we expect that the MoS_2 crystals have degraded through desulfuration. Figure 2b.i,ii shows another pair of images demonstrating the effect of UHV annealing at 1150 °C for 3 h. This treatment further lowers the visibility of the crystals, where they have clearly decomposed, with some residues remaining in triangular shapes. Similar survivor traces have been observed after a lift-off process of WS_2.[29]

STM studies can elucidate the structural transformations at higher resolution than SEM. Below 700 °C, the samples are only degassed; i.e., adsorbates and contaminants are removed. Not much difference is seen after these gentle UHV anneals in STM. The MoS_2 layer is uniform and conforms well to the substrate terraces with a thickness of 0.63 ± 0.06 nm (Figure 3a), which is typical of a monolayer.[1,30] The atomic model of

DOI: 10.1021/acs.jpcc.8b11298
J. Phys. Chem. C 2019, 123, 3876−3885

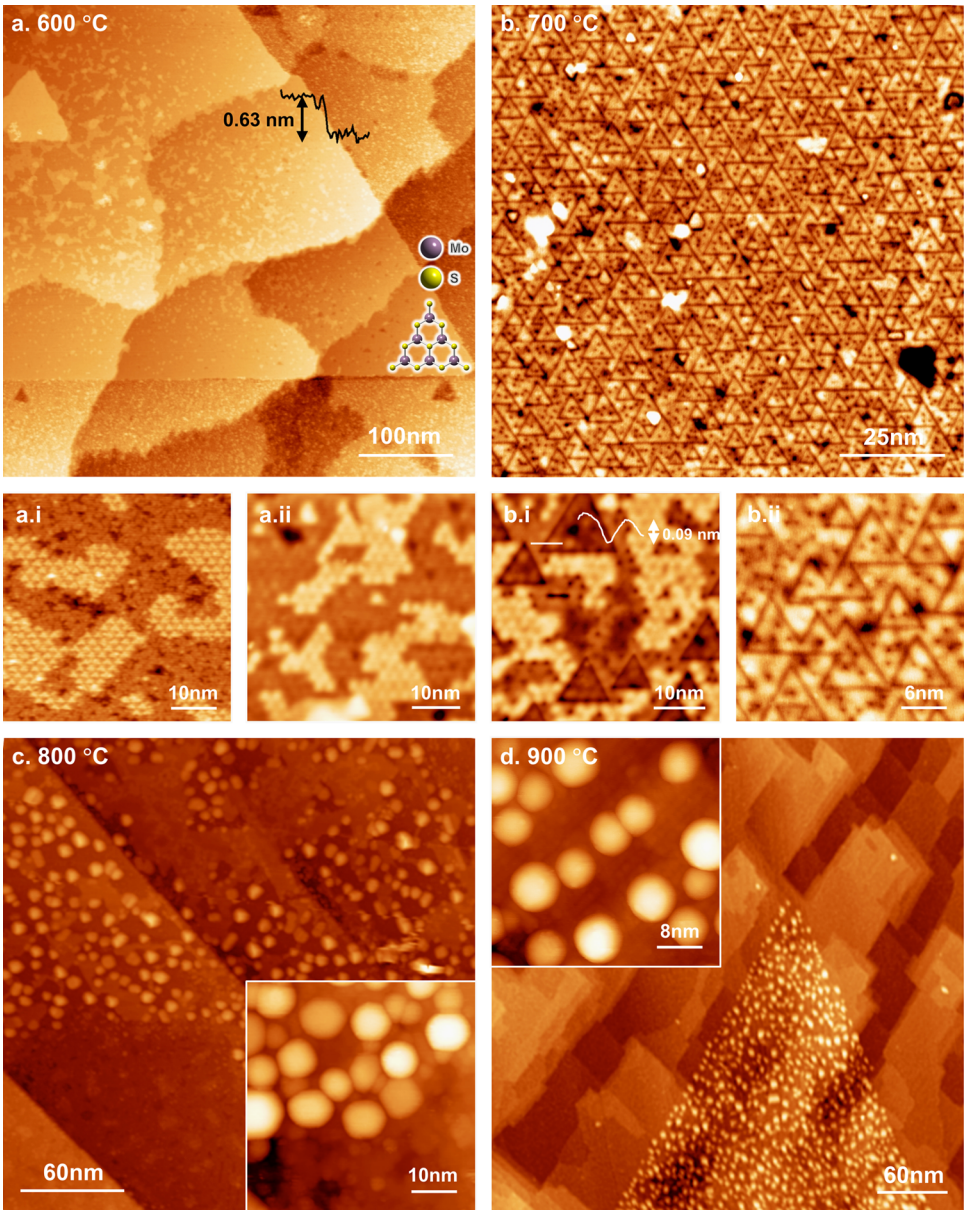

Figure 3. STM images of various stages of the thermal degradation of monolayer MoS_2 crystals. (a) MoS_2 monolayer with a smooth surface up to 600 °C, conforming well to the substrate terraces (V_s = 2.0 V, I_t = 0.05 nA). The monolayer has a typical thickness of 0.63 ± 0.06 nm. The atomic model of MoS_2 overlaid illustrates the lattice orientation, and it also applies to the other panels. (a.i,ii) Zoomed-in images of the morphologies of the $SrTiO_3(111)$ substrate and the MoS_2 monolayer, respectively (a.i: V_s = 2.0 V, I_t = 0.10 nA; a.ii: V_s = 2.0 V, I_t = 0.03 nA). (b) Triangular etch trenches on the MoS_2 monolayer on $SrTiO_3(111)$ formed during UHV annealing at 700 °C (V_s = 2.0 V, I_t = 0.11 nA). (b.ii) Details of the etch trenches (V_s = 2.0 V, I_t = 0.11 nA). (b.i) Area similar to that in (a.ii), for comparison, except for a higher annealing temperature. A line profile across a trench shows a dip of 0.09 nm (V_s = 2.0 V, I_t = 0.03 nA). (c) Degradation of the MoS_2 monolayer into particles while partially retaining the film upon UHV annealing at 800 °C. The substrate is $SrTiO_3(001)$-$c(4 \times 2)$ with straight terraces (V_s = 2.0 V, I_t = 0.05 nA). The inset is a high-magnification image (V_s = 2.0 V, I_t = 0.05 nA). (d) Residual particles left at 900 °C, which remain in the original triangular shape of the MoS_2 crystal, on a $SrTiO_3(110)$-(4×1) substrate (V_s = 2.0 V, I_t = 0.05 nA). The inset shows the details of the residues (V_s = 1.5 V, I_t = 0.20 nA). All images are single scans except (a.ii) and (b.i), which are averaged over 16 and 22 frames by Smart Align,[26] respectively.

MoS_2 overlaid shows the orientation of the triangular crystal, and it also applies to the other panels in Figure 3. The $SrTiO_3(111)$ substrate was processed to generate a (4×4) reconstruction in UHV before the CVD growth of MoS_2;[22,31] although the reconstruction would not have survived in an ambient environment, the terraces still remain. Figure 3a.i,ii shows two high-magnification images illustrating the typical morphologies outside of and on top of the MoS_2 monolayer, respectively. There are clusters of small triangles aligned on the substrate with a periodicity of 2.20 ± 0.05 nm (Figure 3a.i), and these islands are seen to raise the height of the MoS_2 monolayer (Figure 3a.ii). These clusters are believed to be due to an intermediate step during the high-temperature formation of the $SrTiO_3(111)$-(4×4) reconstruction and will not be discussed further.

After being UHV-annealed at 700 °C, the MoS_2 crystals start to degrade and triangular etch trenches appear, as shown in Figure 3b. The trenches are typically measured to be less than 0.1 nm deep. The etch lines run in three directions along the $\langle 2\bar{1}\bar{1}0 \rangle$-type crystallographic directions of MoS_2, which are

DOI: 10.1021/acs.jpcc.8b11298
J. Phys. Chem. C 2019, 123, 3876−3885

the sulfur-terminated edge directions of the triangular MoS_2 crystal (cf. the atomic model of MoS_2 in Figure 3a). The high-magnification image in Figure 3b.ii shows that there are etch dots as well as etch lines. Figure 3b.i shows an area similar to that in Figure 3a.ii but annealed at 700 °C. It has a complex morphology in which the clusters protruding from the substrate are still visible and the triangular etch trenches coexist with them. The etch dots and lines are likely to be due to the preferential evaporation of sulfur from the MoS_2 monolayers.

At UHV annealing temperatures above 800 °C, the MoS_2 crystals decompose into particles. Figure 3c shows a MoS_2 monolayer (on top of $SrTiO_3$(001)-c(4 × 2) substrate terraces) that has partially degraded into particles.[24,32,33] When the annealing temperature exceeds 900 °C, the MoS_2 crystals degrade entirely and only particle residues are observed in place of the original triangular crystals (Figure 3d). Below the particles is the reconstructed $SrTiO_3$(110)-(4 × 1) substrate.[23,34,35] The residual particles are typically 2−5 nm high and 5−10 nm in diameter.

3.2. XPS Analysis. The pristine and thermally decomposed products of MoS_2 crystals were investigated by XPS. Figure 4 shows the core-level spectra from the Mo 3d and S 2p regions of the samples. In each column, from top to bottom, the spectra compare the compositions of differently treated samples, as labeled in the top-right corner of each figure: as-grown FL MoS_2 crystals, as-grown ML MoS_2 crystals, and monolayer MoS_2 crystals UHV-annealed at 700, 800, 900, and 1000 °C.

In the molybdenum spectra (Figure 4a), it can be seen that Mo exists in both the Mo^{6+} and Mo^{4+} ionization states. Both of these ionization states have a doublet peak in their 3d spectra: 235.2 and 232.3 eV correspond to Mo^{6+} $3d_{3/2}$ and Mo^{6+} $3d_{5/2}$, respectively, typical of MoO_3, and[36] 232.1 and 229.2 eV correspond to Mo^{4+} $3d_{3/2}$ and Mo^{4+} $3d_{5/2}$, respectively, typical of MoS_2 and MoO_2.[37−40] It should be noted that the Mo^{6+} $3d_{5/2}$ and Mo^{4+} $3d_{3/2}$ peaks are almost coincident, giving rise to the characteristic three-peak shape of Mo^{6+} and Mo^{4+}.[40] Along with the Mo peaks, another peak observed at 226.3 eV belongs to S 2s.[38] In the sulfur spectra (Figure 4b), the S 2p peaks are observed at 163.2 and 162.0 eV, representing S $2p_{1/2}$ and S $2p_{3/2}$ orbital splitting, respectively.[41]

Interpreting the XPS observations, we can infer that the as-grown samples (marked as "FL" and "ML") are MoS_2 crystals mixed with a small amount of the unreacted MoO_3 precursor and the intermediate product MoO_2.[42] Sulfur completely leaves the structure at a temperature between 700 and 800 °C, when MoS_2 is fully oxidized. At increasingly higher temperatures, the amount of Mo^{6+} increases because more MoO_3 is formed as MoS_2 is oxidized by the $SrTiO_3$ substrate. Afterward, all of the molybdenum oxides evaporate at T > 1000 °C.

The relative amounts of MoO_3, MoO_2, and MoS_2 in various samples are estimated from the areas of the Gaussian curves of Mo^{6+}, Mo^{4+}, and S^{2-} and by using the relative sensitivity values of the different elements reported in the literature.[43] The results are plotted in Figure 5, with the errors estimated from the uncertainties during peak fitting. The FL, ML, and 700 °C UHV-annealed samples have similar amounts of MoO_3, MoO_2, and MoS_2, where the oxides are the unreacted/incompletely reacted precursor.[42] The FL sample has slightly more MoO_3 than the ML sample because it had a larger

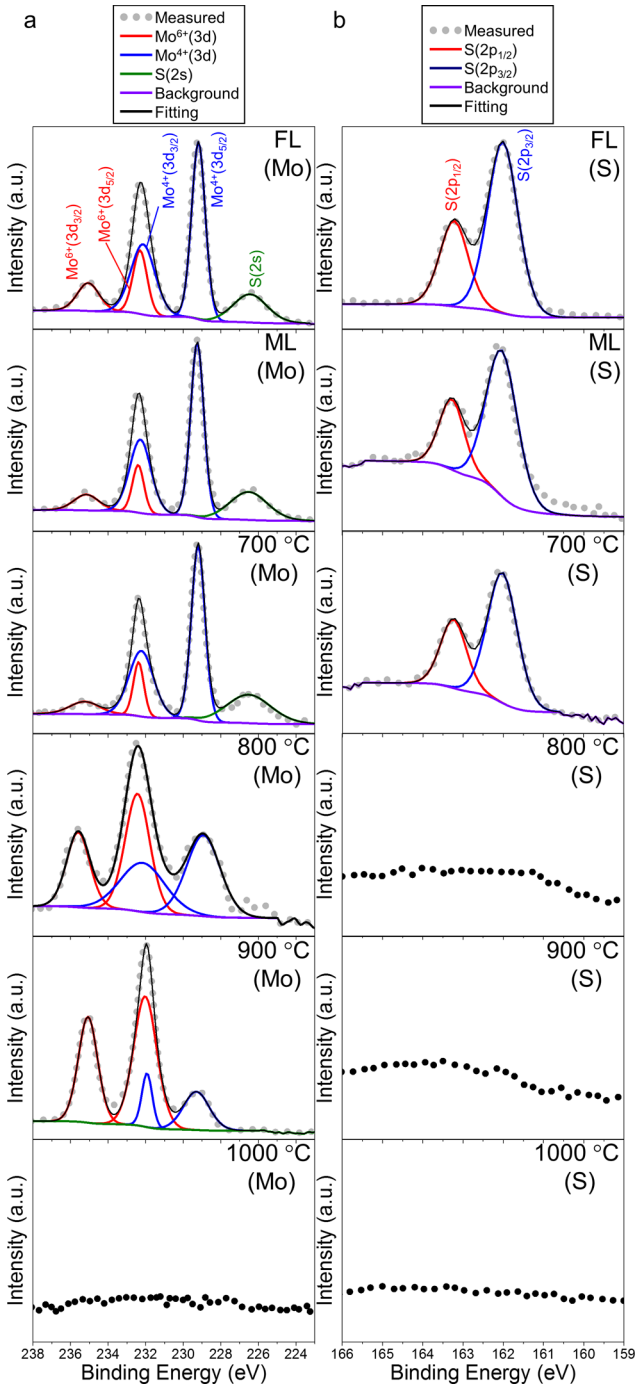

Figure 4. XPS spectra of the (a) Mo 3d and (b) S 2p core-level peaks of the MoS_2 crystals grown on $SrTiO_3$ substrates. From top to bottom: as-grown few-layered (FL) MoS_2 crystals, as-grown monolayered (ML) MoS_2 crystals, and monolayered MoS_2 crystals UHV annealed at 700, 800, 900, and 1000 °C.

amount of precursors deposited. At 700 °C, there is a slightly increased amount of MoO_2 and a virtually unchanged amount of MoO_3 when compared to that of the ML pristine sample. This means that at 700 °C a small but noticeable amount of MoS_2 has been converted into MoO_2 (but not MoO_3 yet). At 800 °C, the % MoS_2 value rapidly decreases to a negligibly small percentage and similar amounts of MoO_2 and MoO_3 are present. At 900 °C, more than 75% of the residue is MoO_3. Therefore, the compositional change is likely to follow the

DOI: 10.1021/acs.jpcc.8b11298
J. Phys. Chem. C 2019, 123, 3876−3885

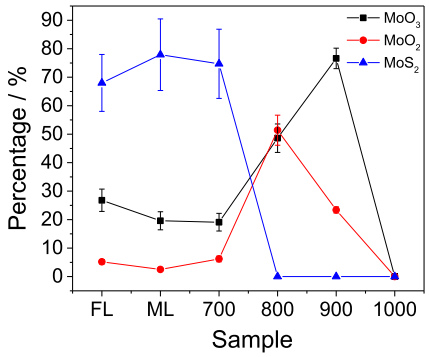

Figure 5. Atomic percentage of substances in the as-grown MoS_2 crystals (few-layered and monolayered) and MoS_2 monolayers UHV-annealed at 700, 800, 900, and 1000 °C.

route $MoS_2 \rightarrow MoO_2 \rightarrow MoO_3$. At $T \geq 1000$ °C, all of the molybdenum compounds have evaporated and to indicate this, the atomic percentages have been set to zero.

3.3. PL and Raman Spectroscopies. To gain further insight into the thermal degradation of MoS_2 crystals, PL and Raman spectroscopies were carried out (Figure 6). Upon laser excitation, the as-grown sample exhibits a strong PL peak at the photon energy of 1.88 eV (black curve in Figure 6a), characteristic of monolayer MoS_2.[3,44−47] In the Raman spectrum (black curve in Figure 6b), there are two peaks at 382.2 and 403.0 cm^{-1}, corresponding to the in-plane E^1_{2g} and out-of-plane A_{1g} vibrational modes of MoS_2, respectively.[48,49] The frequency difference of ∼20 cm^{-1} between the peaks is the signature of MoS_2 monolayers, whereas the difference for thicker and bulk MoS_2 is ∼25 cm^{-1}.[47−52] UHV annealing at 700 °C results in significantly decreased intensities of the PL and Raman peaks (red curves in Figure 6), demonstrating the deteriorated crystallinity of the MoS_2 monolayers. When the UHV annealing temperature reaches 800 °C, no PL or Raman signals can be observed (green curves in Figure 6).

Both PL and Raman peaks have shifted after the samples were UHV-annealed at 700 °C. Before the peak shifts are discussed, it should be mentioned that strains form in the MoS_2 crystals during the fast cooling process in the CVD reactor. This is due to the different thermal expansion coefficients (TECs) of MoS_2 and the $SrTiO_3$ substrate.[53] The TEC of the as-prepared 2H-phase MoS_2 ($\alpha_{MoS_2,a} = 1.9 \times 10^{-6}$ K^{-1} and $\alpha_{MoS_2,c} = 8.65 \times 10^{-6}$ K^{-1}, 293−1073 K) is approximately one order of magnitude smaller than that of $SrTiO_3$ ($\alpha_{SrTiO_3} = 3.23 \times 10^{-5}$ K^{-1}, 300−1800 K).[54,55] This difference introduces compressive strain in the MoS_2 layers on $SrTiO_3$. In addition, there are strains induced by the epitaxial relationship on different terminations of $SrTiO_3$ substrates, which are compressive on $SrTiO_3$(111) and tensile on $SrTiO_3$(001).[28] Overall, MoS_2 crystals on $SrTiO_3$(111) are in compression and those on $SrTiO_3$(001) are in tension.[28]

The post-annealing PL peak position of MoS_2 on $SrTiO_3$(111) shifts to a lower photon energy (red shift), as shown in Figure 6a. This is because the compressive strain in the MoS_2 crystals is partially released; the TEC-induced strain is released by the low heating/cooling rates (2−5 °C min^{-1}) before and after the 700 °C UHV annealing, and the epitaxy-induced strain is released by the degradation of the MoS_2 crystal structure. The red shift could be additionally attributed to more localized states,[10] which in turn are associated with structural defects.[56]

After being UHV-annealed at 700 °C, the Raman peaks of MoS_2 on $SrTiO_3$(001) are both shifted to higher wavenumbers ("stiffening" or blueshifts), accompanied by peak broadening. This is again due to a release of strain, although the strain was initially tensile in the case of a (001)-terminated $SrTiO_3$ substrate.

3.4. Optical Microscopy (OM). UHV annealing up to 1000 °C does not appear to affect the MoS_2 crystal shapes when investigated using only OM. Above 1000 °C, the crystals evaporate and can no longer be seen by OM. Figure 7 shows some MoS_2 crystals on $SrTiO_3$(110) imaged by OM (a) before and (b) after UHV annealing at 1000 °C for 5.5 h. As previously shown, substantial changes occur in the internal structure; the triangles in Figure 7a are pristine MoS_2 crystals, whereas those in Figure 7b are residual MoO_3 nanoparticles retaining the original triangular footprint. However, OM does not show any apparent differences and care should therefore be taken when using OM on its own to describe the quality of MoS_2 crystals.

3.5. Sulfur Annealing. To study whether we could heal the defects formed in the MoS_2 monolayers, we created a sulfur atmosphere in the CVD reactor at an elevated temperature and transported the sulfur vapor to the MoS_2 surface by argon flow. As indicated by SEM, the 700 °C UHV-annealed MoS_2 crystals look similar before (Figure 2a.i) and after (Figure 8a) sulfur annealing. On the other hand, the 800 °C UHV-annealed crystals (Figure 8b) become clear and

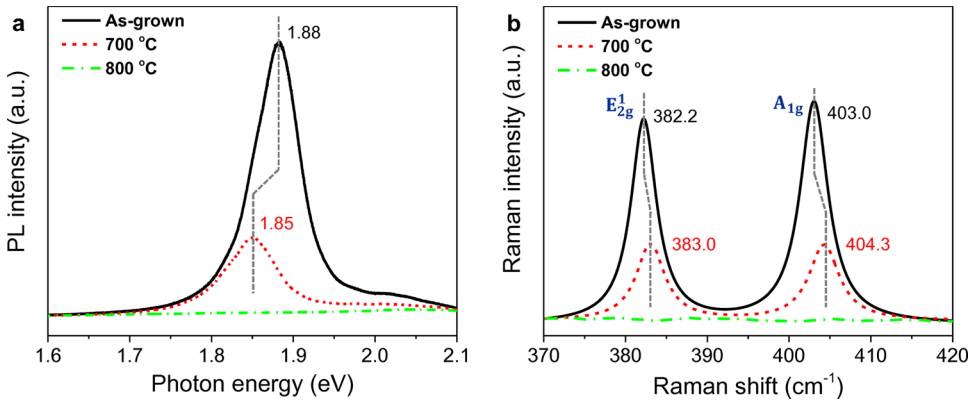

Figure 6. (a) PL spectra of monolayer MoS_2 crystals on $SrTiO_3$(111) and (b) Raman spectra of monolayer MoS_2 crystals on $SrTiO_3$(001): as-grown (black), UHV-annealed at 700 °C (red), and UHV-annealed at 800 °C (green).

DOI: 10.1021/acs.jpcc.8b11298
J. Phys. Chem. C 2019, 123, 3876−3885

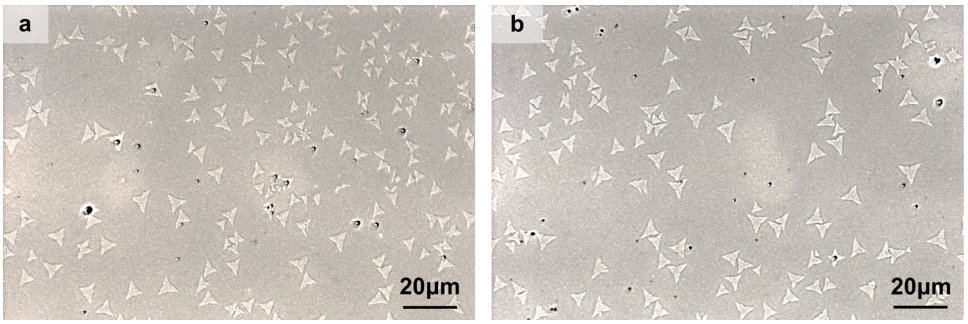

Figure 7. Optical microscope images of MoS_2 crystals on $SrTiO_3(110)$ (a) before and (b) after UHV annealing at 1000 °C for 5.5 h.

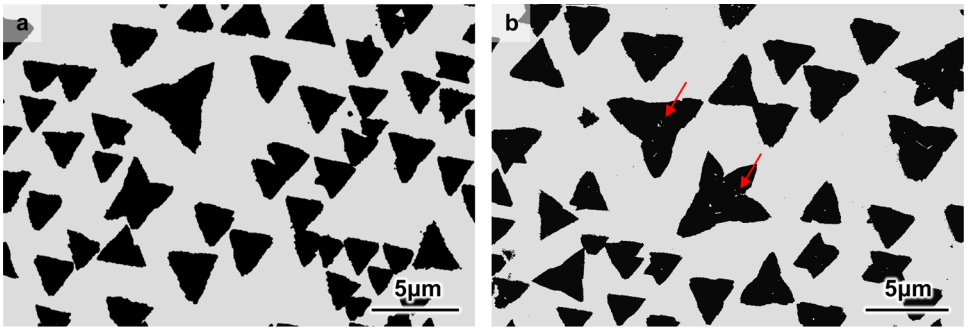

Figure 8. SEM images of (a) 700 °C and (b) 800 °C UHV-annealed MoS_2 crystals on $SrTiO_3(111)$ substrates after sulfur annealing.

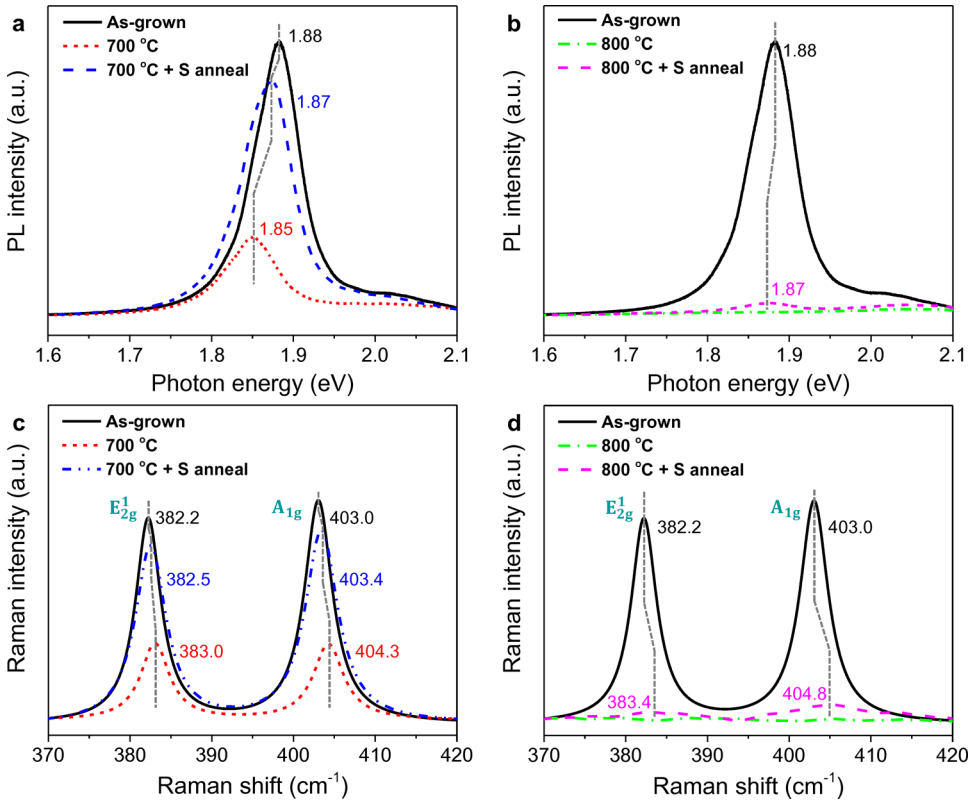

Figure 9. (a, b) PL and (c, d) Raman spectra of the sulfur-annealed MoS_2 crystals compared to those before (i.e., as-grown) and after the UHV annealing at (a, c) 700 °C and (b, d) 800 °C. (a, b) PL spectra are measured on MoS_2 crystals supported on $SrTiO_3(111)$. (c, d) Raman spectra are measured on MoS_2 crystals supported on $SrTiO_3(001)$.

black, with enhanced contrast when compared with the faint triangles in Figure 2a.ii. This indicates partial recovery of the structural degradation. The crystals look similar to the as-grown crystals, although a few more holes are observed in the larger crystals (indicated by red arrows).

The optical properties of the sulfur-annealed samples also partially recover: Figure 9a shows that the PL intensity of the

DOI: 10.1021/acs.jpcc.8b11298
J. Phys. Chem. C 2019, 123, 3876−3885

700 °C UHV-annealed MoS_2 crystal is enhanced and the peak position is blue-shifted back to a higher photon energy, close to that of the newly grown MoS_2 crystals. The Raman signals are also largely restored in terms of the peak intensities and positions (Figure 9c). The peak position restoration is due to the epitaxy-induced strains being reintroduced as the MoS_2 crystallinity improves. The strains are compressive on $SrTiO_3$(111) and tensile on $SrTiO_3$(001),[28] leading to the blue shift of the PL peak in Figure 9a and the red shifts of the Raman peaks in Figure 9c.

On the other hand, after sulfur treatment of the 800 °C UHV-annealed MoS_2 crystals, the recovery of the PL and Raman signals is weak (Figure 9b,d). Also, the frequency difference of 21.4 cm^{-1} between them indicates that the healed MoS_2 is a mixture of ML and FL crystals.[48] Note that the presence of FL MoS_2 crystals is not obvious from the PL peak position at 1.87 eV (Figure 9b), which corresponds to direct excitonic transitions from ML MoS_2 only.[46] This is because the PL signal strength of FL MoS_2 is negligible compared to that of ML MoS_2.[3]

4. DISCUSSION

We now have a deeper understanding of the UHV degradation and healing mechanisms of $SrTiO_3$-supported monolayer MoS_2 crystals, as summarized in Table 1. The structural changes start at 700 °C, which is reflected by the compositional change of the sample at 700 °C compared to that of the pristine ML sample in XPS, where slightly less MoS_2 is present (Figure 5). The desulfurization is not visible in SEM (Figure 2a.i), but the sulfur vacancies appear as etch dots and lines in STM images (Figure 3b). The structural defects are also observed in the decreased PL and Raman intensities (Figure 6). For comparison, previous studies show that when MoS_2 is etched in air at lower temperatures of 300−340 °C,[16,17] triangular surface pits rather than etch lines are the first sign of degradation, suggesting the oxidation of Mo into MoO_3 and the removal of S in a volatile state.[15,18]

Table 1. UHV Thermal Degradation and Sulfur Annealing Results of MoS_2 Crystals on $SrTiO_3$ Substrates

sample	UHV annealing time (h)	morphology	substances (excluding unreacted MoO_3/MoO_2)	recovery of optical properties upon sulfur annealing
FL		smooth crystal	MoS_2	
ML		smooth crystal	MoS_2	
700 °C	0.5−2.0	crystal + etch trenches	MoS_2 (mainly) + MoO_2	near full recovery
800 °C	0.5−2.0	crystal + particles	MoO_2 + MoO_3 (similar amounts)	weak recovery
900 °C	0.5−1.0	particles	MoO_2 + MoO_3 (mainly)	no recovery
1000 °C	2.0−5.5	particles/ evaporated		no recovery

After the 800 °C UHV annealing, XPS results (Figures 4 and 5) demonstrate that no sulfur remains and MoO_2 and MoO_3 are formed as the oxidation products of the remaining Mo. The structural change is visualized via the deteriorated contrast in the SEM image (Figure 2a.ii). No PL and Raman signals of MoS_2 are observed any more (Figure 6). The particles in the STM images (Figure 3c) are therefore MoO_x (x = 2−3) particles. At 900 °C, further oxidation occurs and a larger proportion of MoO_3 (> 75%) is detected by XPS (Figure 5).

In the thermally assisted oxidation of monolayer MoS_2 crystals in air, it has been previously reported that sulfur escapes as SO_2,[15,18] leaving oxidized Mo on the surface.[13−18] The thermal degradation of MoS_2 in UHV is likely to follow a different route from that in an O_2-rich environment. We postulate that at 700 °C the thermal energy breaks the Mo−S covalent bonds and releases the S atoms into the vacuum. This bond-breaking process requires a higher activation temperature compared to that of the oxidation of S in an ambient environment.[13−18] Upon higher-temperature UHV annealing (> 800 °C), the $SrTiO_3$ substrate can supply increasing amounts of oxygen, which oxidizes the remaining Mo, converting it into MoO_2 and then into MoO_3.

The high temperature applied to MoS_2 breaks the Mo−S covalent bonds, which are stronger than the van der Waals (vdW) interaction between the MoS_2 sheet and the substrate by orders of magnitude. This explains the observation that the thermal degradation behavior of MoS_2 on different terminations of $SrTiO_3$ substrates is similar, as only their interfacial vdW interaction with the substrate differs.

Finally, the sulfur annealing process partially heals the MoS_2 crystals, as confirmed by SEM observations (Figure 8) and PL and Raman spectroscopies (Figure 9). This recovery is due to the sulfur vacancies in the MoS_2 crystals being restored in the hot sulfur atmosphere.[10] However, the recovery is not full for the 700/800 °C treated samples and the crystals that were UHV annealed at 900 °C or above could not be healed by sulfur annealing at all. This is because once any Mo has been oxidized, it can no longer be sulfurized under the sulfur annealing conditions, or specifically, at a substrate temperature of 300 °C. The reason for this is that the conversion of MoO_3/MoO_2 into MoS_2 requires a higher reaction temperature of 650−800 °C, as in the CVD growth of MoS_2.[10,42] Also, MoO_3/MoO_2 has to be in the gaseous phase for the sulfurization reaction to occur.[10,42] Although there may be a low vapor pressure of MoO_3/MoO_2 at 300 °C, the high Ar flow rate of 500 sccm would quickly remove any vaporized Mo oxides downstream in the furnace. Therefore, no sulfurization of the Mo oxides occurred during the sulfur annealing and any recovered MoS_2 is due to the filling of sulfur vacancies only. For this process to be possible, the Mo atoms need to have largely remained in their original lattice positions of MoS_2 so that the sulfur atoms can easily fill the vacancies. This is true for the crystals that were UHV annealed at 700 and 800 °C; the former only lost a small amount of sulfur (Figures 4 and 5) and remained as a film with some etch trenches (Figure 3b) and the latter lost all sulfur (Figures 4 and 5) but survived partly as a film (Figure 3c). The more the film structure that survived, the stronger the recovery of the optical properties (Figure 9). Also, after the 800 °C UHV annealing, because the film has partially turned into granules, the recovered MoS_2 has some FL crystals mixed with it, as mentioned at the end of Section 3.5. The partial recovery of the 700/800 °C UHV-annealed samples also tells us that in these samples there is a certain amount of MoS_2 that has lost S but has not been oxidized after UHV annealing. However, in the XPS calculations that produced Figure 5, any Mo^{4+} without S was attributed to MoO_2. The calculations are hence not perfect but remain a good estimate of the relative amounts of MoO_3,

DOI: 10.1021/acs.jpcc.8b11298
J. Phys. Chem. C 2019, 123, 3876−3885

MoO_2, and MoS_2 given the XPS data available. A further issue is that a proportion of Mo that may be present in the metallic state in UHV will become oxidized during the ambient transfer to the XPS chamber.

5. CONCLUSIONS

This study uncovers the thermal degradation behavior of monolayer MoS_2 in UHV because of sulfur loss, which begins at 700 °C. The sulfur vacancies can be filled by annealing the crystals in a hot sulfur atmosphere, and the optical properties of monolayer MoS_2 can nearly be fully recovered. At higher UHV annealing temperatures, the remaining Mo is oxidized by the $SrTiO_3$ substrates into MoO_2 and MoO_3. The sulfur annealing no longer takes effect when all of the Mo has been oxidized, which happens at a temperature between 800 and 900 °C in UHV. The MoS_2 crystal shapes are stable upon annealing until the residual MoO_3 particles evaporate at above 1000 °C. This infers that any triangular crystals that look intact under low-magnification OM and SEM may not mean pristine MoS_2 and OM should be used with care. We conclude that for retaining the properties of MoS_2 it is important to avoid desulfuration and its exposure to oxygen, including the use of oxide substrates. The sulfur vacancies can be restored in a vaporous sulfur environment, whereas the oxidation cannot be reversed. This study provides helpful insights for expanding the high-temperature applications of monolayer MoS_2 crystals in electronics and sensors.

■ AUTHOR INFORMATION

Corresponding Authors

*E-mail: peiyu.chen@materials.ox.ac.uk (P.C.).
*E-mail: martin.castell@materials.ox.ac.uk (M.R.C.).

ORCID

Peiyu Chen: 0000-0002-6877-6142
Jamie H. Warner: 0000-0002-1271-2019

Author Contributions

†P.C. and W.X. contributed equally to this work.

Notes

The authors declare no competing financial interest.

■ ACKNOWLEDGMENTS

The authors would like to thank Chris Spencer (JEOL U.K.) for technical support and Dr Krishnan Murugappan and Jiawei Jiang for taking SEM images on a Zeiss Merlin. J.H.W. acknowledges the support from the Royal Society.

■ REFERENCES

(1) Jiang, C.; Rumyantsev, S. L.; Samnakay, R.; Shur, M. S.; Balandin, A. A. High-Temperature Performance of MoS_2 Thin-Film Transistors: Direct Current and Pulse Current-Voltage Characteristics. *J. Appl. Phys.* **2015**, *117*, No. 064301.

(2) Neudeck, P. G.; Okojie, R. S.; Chen, L.-Y. High-Temperature Electronics—A Role for Wide Bandgap Semiconductors? *Proc. IEEE* **2002**, *90*, 1065−1076.

(3) Mak, K. F.; Lee, C.; Hone, J.; Shan, J.; Heinz, T. F. Atomically Thin MoS_2: A New Direct-Gap Semiconductor. *Phys. Rev. Lett.* **2010**, *105*, No. 136805.

(4) Fivaz, R.; Mooser, E. Mobility of Charge Carriers in Semiconducting Layer Structures. *Phys. Rev.* **1967**, *163*, 743−755.

(5) Lee, G.-H.; Yu, Y.-J.; Cui, X.; Petrone, N.; Lee, C.-H.; Choi, M. S.; Lee, D.-Y.; Lee, C.; Yoo, W. J.; Watanabe, K.; et al. Flexible and Transparent MoS_2 Field-Effect Transistors on Hexagonal Boron Nitride-Graphene Heterostructures. *ACS Nano* **2013**, *7*, 7931−7936.

(6) Marx, M.; Nordmann, S.; Knoch, J.; Franzen, C.; Stampfer, C.; Andrzejewski, D.; Kümmell, T.; Bacher, G.; Heuken, M.; Kalisch, H.; et al. Large-Area MoS_2 Deposition via MOVPE. *J. Cryst. Growth* **2017**, *464*, 100−104.

(7) Lamouchi, A.; Assaker, I. B.; Chtourou, R. Effect of Annealing Temperature on the Structural, Optical, and Electrical Properties of MoS_2 Electrodeposited onto Stainless Steel Mesh. *J. Mater. Sci.* **2017**, *52*, 4635−4646.

(8) Barvat, A.; Prakash, N.; Satpati, B.; Singha, S. S.; Kumar, G.; Singh, D. K.; Dogra, A.; Khanna, S. P.; Singha, A.; Pal, P. Emerging Photoluminescence from Bilayer Large-Area 2D MoS_2 Films Grown by Pulsed Laser Deposition on Different Substrates. *J. Appl. Phys.* **2017**, *122*, No. 015304.

(9) Kaindl, R.; Bayer, B. C.; Resel, R.; Müller, T.; Skakalova, V.; Habler, G.; Abart, R.; Cherevan, A. S.; Eder, D.; Blatter, M.; et al. Growth, Structure and Stability of Sputter-Deposited MoS_2 Thin Films. *Beilstein J. Nanotechnol.* **2017**, *8*, 1115−1126.

(10) Xu, W.; Li, S.; Zhou, S.; Lee, J. K.; Wang, S.; Sarwat, S. G.; Wang, X.; Bhaskaran, H.; Pasta, M.; Warner, J. H. Large Dendritic Monolayer MoS_2 Grown by Atmospheric Pressure Chemical Vapor Deposition for Electrocatalysis. *ACS Appl. Mater. Interfaces* **2018**, *10*, 4630−4639.

(11) Heo, S.; Hayakawa, R.; Wakayama, Y. Carrier Transport Properties of MoS_2 Field-Effect Transistors Produced by Multi-Step Chemical Vapor Deposition Method. *J. Appl. Phys.* **2017**, *121*, No. 024301.

(12) Ahn, J.-H.; Parkin, W. M.; Naylor, C. H.; Johnson, A. T. C.; Drndić, M. Ambient Effects on Electrical Characteristics of CVD-Grown Monolayer MoS_2 Field-Effect Transistors. *Sci. Rep.* **2017**, *7*, No. 4075.

(13) Budania, P.; Baine, P. T.; Montgomery, J. H.; McNeill, D. W.; Mitchell, S. J. N.; Modreanu, M.; Hurley, P. K. Effect of Post-Exfoliation Treatments on Mechanically Exfoliated MoS_2. *Mater. Res. Express* **2017**, *4*, No. 025022.

(14) Ponomarev, E. A.; Neumann-Spallart, M.; Hodes, G.; Lévy-Clément, C. Electrochemical Deposition of MoS_2 Thin Films by Reduction of Tetrathiomolybdate. *Thin Solid Films* **1996**, *280*, 86−89.

(15) Windom, B. C.; Sawyer, W. G.; Hahn, D. W. A Raman Spectroscopic Study of MoS_2 and MoO_3: Applications to Tribological Systems. *Tribol. Lett.* **2011**, *42*, 301−310.

(16) Wu, J.; Li, H.; Yin, Z.; Li, H.; Liu, J.; Cao, X.; Zhang, Q.; Zhang, H. Layer Thinning and Etching of Mechanically Exfoliated MoS_2 Nanosheets by Thermal Annealing in Air. *Small* **2013**, *9*, 3314−3319.

(17) Yamamoto, M.; Einstein, T. L.; Fuhrer, M. S.; Cullen, W. G. Anisotropic Etching of Atomically Thin MoS_2. *J. Phys. Chem. C* **2013**, *117*, 25643−25649.

(18) Bandaru, N.; Kumar, R. S.; Sneed, D.; Tschauner, O.; Baker, J.; Antonio, D.; Luo, S.-N.; Hartmann, T.; Zhao, Y.; Venkat, R. Effect of Pressure and Temperature on Structural Stability of MoS_2. *J. Phys. Chem. C* **2014**, *118*, 3230−3235.

(19) Grønborg, S. S.; Ulstrup, S.; Bianchi, M.; Dendzik, M.; Sanders, C. E.; Lauritsen, J. V.; Hofmann, P.; Miwa, J. A. Synthesis of Epitaxial Single-Layer MoS_2 on Au(111). *Langmuir* **2015**, *31*, 9700−9706.

(20) Liu, D.; Chen, X.; Li, D.; Wang, F.; Luo, X.; Yang, B. Simulation of MoS_2 Crystal Structure and the Experimental Study of Thermal Decomposition. *J. Mol. Struct.* **2010**, *980*, 66−71.

(21) Noland, J. A. Optical Absorption of Single-Crystal Strontium Titanate. *Phys. Rev.* **1954**, *94*, No. 724.

(22) Russell, B. C.; Castell, M. R. Surface of Sputtered and Annealed Polar $SrTiO_3$(111): TiO_x-Rich (n × n) Reconstructions. *J. Phys. Chem. C* **2008**, *112*, 6538−6545.

(23) Russell, B. C.; Castell, M. R. Reconstructions on the Polar $SrTiO_3$(110) Surface: Analysis Using STM, LEED, and AES. *Phys. Rev. B* **2008**, *77*, No. 245414.

(24) Castell, M. R. Scanning Tunneling Microscopy of Reconstructions on the $SrTiO_3$(001) Surface. *Surf. Sci.* **2002**, *505*, 1−13.

DOI: 10.1021/acs.jpcc.8b11298
J. Phys. Chem. C 2019, 123, 3876−3885

(25) Jones, L.; Yang, H.; Pennycook, T. J.; Marshall, M. S. J.; Van Aert, S.; Browning, N. D.; Castell, M. R.; Nellist, P. D. Smart Align—A New Tool for Robust Non-Rigid Registration of Scanning Microscope Data. *Adv. Struct. Chem. Imag.* **2015**, *1*, No. 8.
(26) Jones, L.; Wang, S.; Hu, X.; ur Rahman, S.; Castell, M. R. Maximising the Resolving Power of the Scanning Tunneling Microscope. *Adv. Struct. Chem. Imag.* **2018**, *4*, No. 7.
(27) Horcas, I.; Fernández, R.; Gómez-Rodríguez, J. M.; Colchero, J.; Gómez-Herrero, J.; Baro, A. M. WSXM: A Software for Scanning Probe Microscopy and a Tool for Nanotechnology. *Rev. Sci. Instrum.* **2007**, *78*, No. 013705.
(28) Chen, P.; Xu, W.; Gao, Y.; Warner, J. H.; Castell, M. R. Epitaxial Growth of Monolayer MoS_2 on $SrTiO_3$ Single Crystal Substrates. *ACS Appl. Nano Mater.* **2018**, *1*, 6976−6988.
(29) Sheng, Y.; Xu, W.; Wang, X.; He, Z.; Rong, Y.; Warner, J. H. Mixed Multilayered Vertical Heterostructures Utilizing Strained Monolayer WS_2. *Nanoscale* **2016**, *8*, 2639−2647.
(30) Radisavljevic, B.; Radenovic, A.; Brivio, J.; Giacometti, V.; Kis, A. Single-Layer MoS_2 Transistors. *Nat. Nanotechnol.* **2011**, *6*, 147−150.
(31) Marks, L. D.; Chiaramonti, A. N.; ur Rahman, S.; Castell, M. R. Transition from Order to Configurational Disorder for Surface Reconstructions on $SrTiO_3(111)$. *Phys. Rev. Lett.* **2015**, *114*, No. 226101.
(32) Becerra-Toledo, A. E.; Marshall, M. S. J.; Castell, M. R.; Marks, L. D. $c(4 \times 2)$ and Related Structural Units on the $SrTiO_3(001)$ Surface: Scanning Tunneling Microscopy, Density Functional Theory, and Atomic Structure. *J. Chem. Phys.* **2012**, *136*, No. 214701.
(33) Erdman, N.; Warschkow, O.; Asta, M.; Poeppelmeier, K. R.; Ellis, D. E.; Marks, L. D. Surface Structures of $SrTiO_3$ (001): A TiO_2-Rich Reconstruction with a $c(4 \times 2)$ Unit Cell. *J. Am. Chem. Soc.* **2003**, *125*, 10050−10056.
(34) Enterkin, J. A.; Subramanian, A. K.; Russell, B. C.; Castell, M. R.; Poeppelmeier, K. R.; Marks, L. D. A Homologous Series of Structures on the Surface of $SrTiO_3(110)$. *Nat. Mater.* **2010**, *9*, 245−248.
(35) Wang, Z.; Loon, A.; Subramanian, A.; Gerhold, S.; McDermott, E.; Enterkin, J. A.; Hieckel, M.; Russell, B. C.; Green, R. J.; Moewes, A.; et al. Transition from Reconstruction toward Thin Film on the (110) Surface of Strontium Titanate. *Nano Lett.* **2016**, *16*, 2407−2412.
(36) Qin, P.; Fang, G.; Ke, W.; Cheng, F.; Zheng, Q.; Wan, J.; Lei, H.; Zhao, X. In Situ Growth of Double-Layer MoO_3/MoS_2 Film from MoS_2 for Hole-Transport Layers in Organic Solar Cell. *J. Mater. Chem. A* **2014**, *2*, 2742−2756.
(37) Jiang, L.; Zhang, S.; Kulinich, S. A.; Song, X.; Zhu, J.; Wang, X.; Zeng, H. Optimizing Hybridization of 1T and 2H Phases in MoS_2 Monolayers to Improve Capacitances of Supercapacitors. *Mater. Res. Lett.* **2015**, *3*, 177−183.
(38) Kumar, P.; Singh, M.; Sharma, R. K.; Reddy, G. B. A Study on Role of Partial Pressure in Controlled Synthesis of Core-Shell MoO_2/MoS_2 Nanoflakes. *Mater. Chem. Phys.* **2016**, *178*, 6−11.
(39) Sun, Y.; Hu, X.; Luo, W.; Huang, Y. Ultrafine MoO_2 Nanoparticles Embedded in a Carbon Matrix as a High-Capacity and Long-Life Anode for Lithium-Ion Batteries. *J. Mater. Chem.* **2012**, *22*, 425−431.
(40) Jin, Y.; Shen, P. K. Nanoflower-Like Metallic Conductive MoO_2 as a High-Performance Non-Precious Metal Electrocatalyst for the Hydrogen Evolution Reaction. *J. Mater. Chem. A* **2015**, *3*, 20080−20085.
(41) Shi, Y.; Huang, J.-K.; Jin, L.; Hsu, Y.-T.; Yu, S. F.; Li, L.-J.; Yang, H. Y. Selective Decoration of Au Nanoparticles on Monolayer MoS_2 Single Crystals. *Sci. Rep.* **2013**, *3*, No. 1839.
(42) Pondick, J. V.; Woods, J. M.; Xing, J.; Zhou, Y.; Cha, J. J. Stepwise Sulfurization from MoO_3 to MoS_2 via Chemical Vapor Deposition. *ACS Appl. Nano Mater.* **2018**, *1*, 5655−5661.
(43) Briggs, D.; Seah, M. P. *Practical Surface Analysis: Auger and X-ray Photoelectron Spectroscopy*; John Wiley & Sons: NY, 1990.
(44) Dhakal, K. P.; Duong, D. L.; Lee, J.; Nam, H.; Kim, M.; Kan, M.; Lee, Y. H.; Kim, J. Confocal Absorption Spectral Imaging of MoS_2: Optical Transitions Depending on the Atomic Thickness of Intrinsic and Chemically Doped MoS_2. *Nanoscale* **2014**, *6*, 13028−13035.
(45) Zhou, X.; Kang, K.; Xie, S.; Dadgar, A.; Monahan, N. R.; Zhu, X.-Y.; Park, J.; Pasupathy, A. N. Atomic-Scale Spectroscopy of Gated Monolayer MoS_2. *Nano Lett.* **2016**, *16*, 3148−3154.
(46) Splendiani, A.; Sun, L.; Zhang, Y.; Li, T.; Kim, J.; Chim, C.-Y.; Galli, G.; Wang, F. Emerging Photoluminescence in Monolayer MoS_2. *Nano Lett.* **2010**, *10*, 1271−1275.
(47) Ling, X.; Lee, Y.-H.; Lin, Y.; Fang, W.; Yu, L.; Dresselhaus, M. S.; Kong, J. Role of the Seeding Promoter in MoS_2 Growth by Chemical Vapor Deposition. *Nano Lett.* **2014**, *14*, 464−472.
(48) Lee, C.; Yan, H.; Brus, L. E.; Heinz, T. F.; Hone, J.; Ryu, S. Anomalous Lattice Vibrations of Single- and Few-Layer MoS_2. *ACS Nano* **2010**, *4*, 2695−2700.
(49) Li, H.; Zhang, Q.; Yap, C. C. R.; Tay, B. K.; Edwin, T. H. T.; Olivier, A.; Baillargeat, D. From Bulk to Monolayer MoS_2: Evolution of Raman Scattering. *Adv. Funct. Mater.* **2012**, *22*, 1385−1390.
(50) Eda, G.; Yamaguchi, H.; Voiry, D.; Fujita, T.; Chen, M.; Chhowalla, M. Photoluminescence from Chemically Exfoliated MoS_2. *Nano Lett.* **2011**, *11*, 5111−5116.
(51) Wang, S.; Rong, Y.; Fan, Y.; Pacios, M.; Bhaskaran, H.; He, K.; Warner, J. H. Shape Evolution of Monolayer MoS_2 Crystals Grown by Chemical Vapor Deposition. *Chem. Mater.* **2014**, *26*, 6371−6379.
(52) Yu, Y.; Li, C.; Liu, Y.; Su, L.; Zhang, Y.; Cao, L. Controlled Scalable Synthesis of Uniform, High-Quality Monolayer and Few-Layer MoS_2 Films. *Sci. Rep.* **2013**, *3*, No. 1866.
(53) Liu, Z.; Amani, M.; Najmaei, S.; Xu, Q.; Zou, X.; Zhou, W.; Yu, T.; Qiu, C.; Birdwell, A. G.; Crowne, F. J.; et al. Strain and Structure Heterogeneity in MoS_2 Atomic Layers Grown by Chemical Vapour Deposition. *Nat. Commun.* **2014**, *5*, No. 5246.
(54) El-Mahalawy, S. H.; Evans, B. L. The Thermal Expansion of 2H-MoS_2, 2H-$MoSe_2$ and 2H-WSe_2 between 20 and 800 °C. *J. Appl. Crystallogr.* **1976**, *9*, 403−406.
(55) de Ligny, D.; Richet, P. High-Temperature Heat Capacity and Thermal Expansion of $SrTiO_3$ and $SrZrO_3$ Perovskites. *Phys. Rev. B* **1996**, *53*, 3013−3022.
(56) Qiu, H.; Xu, T.; Wang, Z.; Ren, W.; Nan, H.; Ni, Z.; Chen, Q.; Yuan, S.; Miao, F.; Song, F.; et al. Hopping Transport Through Defect-Induced Localized States in Molybdenum Disulphide. *Nat. Commun.* **2013**, *4*, No. 2642.

DOI: 10.1021/acs.jpcc.8b11298
J. Phys. Chem. C 2019, 123, 3876−3885